Preparation And Adsorption Performance of Nano-Hydroxyapatite-Enhanced Acrylamide Hydrogel Adsorbent

Zhi-Ke Wang
TGU: Tiangong University
Ting-Ting Li
TGU: Tiangong University
Hao-Kai Peng
TGU: Tiangong University
Hai-Tao Ren
TGU: Tiangong University
Ching-Wen Lou
Asia University
Jia-Horng Lin (jhlin@fcu.edu.tw)
Feng Chia University https://orcid.org/0000-0002-6913-8986

Research Article

Keywords: adsorption, hydrogel, mechanical properties, composites, kinetics (polym.)

Posted Date: August 31st, 2021

DOI: https://doi.org/10.21203/rs.3.rs-834895/v1

Abstract

In this study, a hydrogel adsorbent was successfully synthesized using hydroxyapatite/acrylamide/β-cyclodextrin to adsorb heavy metal ions and dyes in water. In the study, different contents of hydroxyapatite were added to the hydrogel, and then the mechanical properties and adsorption properties of the material were studied. The results show that the compressive strength of hydrogel added with hydroxyapatite increased by 37.1%. According to the adsorption isotherm model, the maximum adsorption capacity is 300mg/g. In addition, the preparation process of the composite hydrogel is simple, and can be used at a lower pH value, and can be used multiple times. Therefore, the material is of great significance to the treatment of pollutants.

Introduction

At present, heavy metals and industrial dyes are the main pollutants of water resources in many parts of the world. Industrial activities have caused a large amount of organic and inorganic printing and dyeing wastewater. These pollutants can cause genetic and physiological problems in organisms [1, 2]. At present, there are many methods to deal with toxic substances, such as: chemical deposition, ion exchange, electrochemical removal, adsorption, coagulation, flocculation, membrane separation and other methods [3-6].

The adsorption method is superior to other methods due to its low cost, simple design and high efficiency. It is widely used due to its simplicity and high efficiency. However, it is difficult for traditional adsorbents to treat toxic substances in wastewater to a safe level [7-9]. Hydrogels are the latest adsorbents used to treat pollutants in recent years [10, 11]. They have good mechanical properties and are easy to use and reuse [12]. Therefore, the hydrogel has found a special location in the field of wastewater treatment [13]. At present, the main materials of synthetic hydrogels are natural polymers or synthetic polymers: inorganic clay, cellulose, acrylic acid and graphene oxide [14-16]. Hydroxyapatite widely exists in nature and is used in medical field because of its unique compatibility [17-19]. In addition, hydroxyapatite has a large number of active groups, which can adsorb toxic substances in the medium in the form of ion exchange, coordination and hydrogen bond, so it is also used as an adsorbent [20, 21].

In this study, hydroxyapatite and acrylamide / cyclodextrin / polyvinyl alcohol were used to synthesize a hydrogel adsorbent. The influence of inorganic material hydroxyapatite on hydrogel adsorbent was discussed. In this study, the mechanical properties and adsorption properties of hydrogels were characterized and tested, and the effects of hydroxyapatite on the properties of hydrogels were also discussed.

Materials And Methods

2.1. Materials

Acrylic acid, acrylamide, melamine and paraformaldehyde were purchased from Tianjin Kairuisi Fine Chemical Co., Ltd (Tianjin China); Polyvinyl alcohol (PVA) and Dimethyl Sulfoxide (DMSO) purchased from Shanghai Aladdin Biochemical Technology Co., Ltd(Shanghai China); N,N'- methylenebisacrylamide (MBA), potassium peroxodisulfate (KPS), $Ni(NO_3)_2$, Pb $(NO_3)_2$, β-cyclodextrin, epichlorohydrin(ECH), NaOH, all purchased from Tianjin Jiangtian chemical(Tianjin China)Hydroxyapatite was purchased from Shengan Biotechnology (China), with a particle size of 10±1μm. The physical diagrams of the three clays are shown in Figure 1.

2.2 Hydrogel preparation

First, prepare a 10w/w% polyvinyl alcohol solution under the condition of 90℃. Subsequently, 1%, 3% and 5% of its mass of hydroxyapatite were added to the PVA solution. Dissolve 2g β-cyclodextrin, 2ml acrylic acid, 2g acrylamide and 30mg MBA in 5ml deionized water, then add the mixed solution to 20ml PVA solution containing hydroxyapatite and stir evenly, and finally add to the mixed solution 15mg of KPS. Nitrogen protection is used during the preparation process, and the mixed solution is placed in a vacuum drying oven at 60°C for 2 hours. Finally, using 20 mL DMSO as the solvent, 4mL epichlorohydrin was dissolved in DMSO and 2g sodium hydroxide was added. Then the hydrogel was impregnated in the mixed solution and kept at 60℃ for 1h to obtain the hydroxyapatite composite hydrogel. The physical diagram of the sample is shown in Figure 2.

2.3. Characterizations

The thermal stability of the hydrogel is tested with a thermogravimetric analyzer (TG 209F3, NETZSCH, Bavaria, Germany); Analyze samples with Fourier infrared spectrometer (Thermo Scientific Nicolet 380 FT-IR Fourier spectrometer). The Instron 5969 (Instron, US) was used to compress the hydrogel and the compression rate was 300mm/min. Use flame atomic absorption spectrometer (PerkinElmer AA900) to test the ion concentration of lead ions and nickel ions; Use UV spectrophotometer (UV-2600) to measure the concentration of methylene blue; X-ray photoelectron spectroscopy (Thermo Fisher Scientific ESCALAB 250Xi) measures the change of atomic energy before and after adsorption of the material. The swelling experiment of the hydrogel was measured by gravity method. Under certain conditions (pH=7, T=25℃), it swelled from the absolute dry state to the swelling equilibrium state. All samples were measured 3 times and the average value was taken. The swelling rate (SR) of the hydrogel is calculated using Equation 1:

$$SR = \frac{W_t - W_d}{W_d} \quad (1)$$

Where W_t is the mass of the hydrogel for swelling time t, and W_d is the mass of the absolutely dry hydrogel.

2.4. Sorption experiments

For the adsorption performance of the hydrogel materials for pollutants, this study conducted a series of adsorption experiments using two heavy metal ions and methylene blue. Prepare a Ni(II) and Pb(II) solution with a concentration of 1g/L for standby; configure a 1g/L methylene blue solution for standby. The adsorption capacity (Q_e) of the material for ions can be expressed by Equation (2) as follows:

$$Q_e = \frac{(C_0 - C_e) \times V}{m} \quad (2)$$

where C_0 and C_e are the initial and final concentrations (mg/L) of Pb(II) and Ni(II), V is the volume of the solution (mL), and m is the weight of the adsorbent (mg).

In order to study the effect of pH and sodium ion on the performance of adsorption, HCl (1 M) or NaOH (1 M) were used to adjust the pH value of the solution of the two ions to range from 2 to 7. The initial concentration of both ions is 50mg/L. The adsorption properties of hydrogels were tested at different temperatures and their adsorption models were fitted.

In order to evaluate the recyclable properties of hydrogels, the Pb(II) and Ni(II) adsorbents were eluted with 0.1 M HCl solution and then treated with 0.1 M NaOH solution. The methylene blue was desorbed by hydrochloric acid and anhydrous methanol solution with a concentration of 0.1 mol/L. Finally, deionized water was used to wash the adsorbents.

Results And Discussion

3.1. Characterizations

Figure 3a is the infrared analysis spectrum of the hydroxyapatite composite hydrogel. The -C=O stretching vibration peaks of the carboxyl group of acrylic acid and the amide group of acrylamide at 1727 and 1649cm^{-1} respectively correspond to the bending vibration of -NH- at 1025cm^{-1} [22-24]; The peaks at 3100-3400cm^{-1} and 1090cm^{-1} correspond to the -OH stretching vibration and -CO- stretching vibration of polyvinyl alcohol [25]. The main functional groups of β-cyclodextrin mostly overlap with the characteristic peaks of PVA. The -PO_4 characteristic peak of hydroxyapatite at 1030 cm^{-1} is basically covered by the amino characteristic peak of acrylamide, and the characteristic peak of -OH near 3300 cm^{-1} [26]. The combination of hydroxyapatite and hydrogel does not affect the characteristic functional groups of the hydrogel. Figure 3b shows the thermogravimetric analysis of the four hydrogels. It can be seen that the hydroxyapatite composite hydrogel is relatively stable below 200°C. The swelling rate is an important parameter of the hydrogel used in water treatment. Figure 3c shows the swelling rate before and after adding hydroxyapatite to the hydrogel. As can be seen in Figure 3b, the swelling rate of the hydrogel after adding hydroxyapatite decreased (from 180% to 167%), and the swelling rate decreased with the increase of clay. Since hydroxyapatite can adhere to the long polymer chain, the pores of the three-dimensional structure formed by PVA and PAA are reduced, and the space for filling free water is reduced, so that the swelling rate of the hydrogel is gradually reduced.

Figure 3d shows the compression resilience curves of three Hydroxyapatite-hydrogels at 50% strain. First, the addition of hydroxyapatite improves the compressive strength of the hydrogel. The integral area of the compression rebound curve represents the internal friction dissipation during compression. The smaller the area, the better the elasticity of the hydrogel, so the introduction of hydroxyapatite reduces the elasticity of the hydrogel. Figure 3d shows the maximum compressive strength of the hydroxyapatite composite hydrogel. It can be seen that the greater the amount of hydroxyapatite added, the greater the strength of the hydrogel. From the results, hydroxyapatite improves the compressive strength of the hydrogel the most (37.1%). The crystal structure of hydroxyapatite belongs to the hexagonal crystal system, and the OH^- in it can form hydrogen bonds with the hydroxyl group of PVA, and its nanoparticles can adhere to the three-dimensional framework of PVA and polyacrylic acid, and have a certain cross-linking effect on the long chain of PVA and polyacrylic acid [26].

3.2 Adsorption study

3.2.1. Effect of environmental conditions

Figure 4 (a-c) shows the effect of changing the pH of the system on the removal of Pb(II) and Ni(II) ions and MB by the hydroxyapatite composite hydrogel. It can be seen that as the pH value of the system increases from 2 to 6, the removal efficiency of the hydrogel for pollutants gradually increases, and the adsorption equilibrium is finally reached. When pH<2, the removal efficiency of the adsorbent for the two ions is low. Due to the occurrence of protonation (ie $-NH_2+H^+ \rightarrow -NH_3^+$ or $-COO-+H^+ \rightarrow -COOH$) [27], the removal efficiency is low. Subsequently, the adsorption of lead ions and nickel ions reached adsorption equilibrium at pH=3, and the adsorption of MB reached adsorption equilibrium at pH=4.5, which may mean that the adsorption principles of metal ions and methylene blue are different. It can be seen from Figure 3d that the pH_{PZC} of the hydrogel is 8.12, and the pH_{PZC} of the hydroxyapatite composite hydrogel is 7.43. This means that the positive charge on the surface of the hydrogel is reduced after adding hydroxyapatite, which facilitates the adsorption of cations [17]. It is worth noting that at a lower pH, the composite material has a higher removal efficiency for the two metal ions. At this time, there is still a large amount of positive charges in the system, which is not conducive to the adsorption of metal ions. The reason may be that the large amount of metal ions in the hydrogel The electron-rich group adsorbs heavy metal ions in a coordinated manner[14].

3.2.2 Adsorption kinetics

Figure 5 shows the time curve of the adsorption of two metal ions and methylene blue by the hydrogel. It can be seen that in the initial stage of adsorption, the removal efficiency of the two metal ions increased rapidly and reached equilibrium within the next 50 minutes. The adsorption of metal ions reached equilibrium faster than the adsorption of methyl blue. In the initial stage of adsorption, the hydrogel contains a large number of adsorption sites provided by polar groups, such as hydroxyl, carboxyl, and amino groups, so the concentration of pollutants decreases rapidly. In order to better understand the relationship between time and adsorption rate, use the pseudo-first-level model and pseudo-second-level

model to fit the kinetic data and analyze the equilibrium time data (supporting information, equation 1-2) [28-30]. The adsorption kinetics are summarized in Table 1. It can be seen from Fig. 5 and table 1 that, compared with the pseudo first-order kinetic model, the fitting correlation coefficient R^2 of the pseudo second-order kinetic model is higher than 0.985, and the fitting results of Pb (II) and Ni (II) are more in line with the pseudo second-order kinetic model, which can also better explain the relationship between time and adsorption rate in the adsorption process, The results show that the adsorption rate limiting step may be chemical adsorption or coordination adsorption involving shared valence bonds through electron exchange. The fitting result of the composite hydrogel's adsorption data of methylene blue accords with the pseudo-first-order kinetic model, which indicates that the adsorption mechanism of the dye is different from that of the metal ion. From the perspective of the adsorption rate constant, the crystal structure of hydroxyapatite will affect the adsorption of metal ions by the hydrogel. The adsorption rate depends not only on the content of functional groups, but also on the structure of the material.

Table 1 Hydroxyapatite-hydrogel adsorption kinetic model fitting parameters.

		C_0	Pseudo-first-order			Pseudo-second-order		
		(mg/L)	k_1 (L/min)	Q_e (mg/g)	R^2	k_2 (g/(mg h))	$Q_{e,}$ (mg/g)	R^2
	Pb	50	0.052	46.58	0.9639	0.090	46.58	0.9639
		100	0.049	95.76	0.9716	0.041	95.76	0.9716
1%	Ni	50	0.036	46.91	0.9773	0.050	53.87	0.9915
		100	0.025	97.69	0.9828	0.016	115.26	0.9909
	MB	50	0.031	48.36	0.9944	0.037	56.66	0.9812
		100	0.031	98.23	0.9978	0.019	114.74	0.9882
	Pb	50	0.037	47.70	0.9742	0.052	54.36	0.9913
		100	0.042	97.12	0.9746	0.030	109.48	0.9878
3%	Ni	50	0.056	46.84	0.9585	0.083	52.22	0.9831
		100	0.026	99.15	0.9696	0.017	115.48	0.9826
	MB	50	0.033	48.53	0.9934	0.040	56.31	0.9818
		100	0.033	97.91	0.9962	0.020	113.59	0.9875
	Pb	50	0.059	47.46	0.9614	0.092	52.32	0.9856
		100	0.049	95.76	0.9716	0.037	106.76	0.9884
5%	Ni	50	0.044	47.80	0.9853	0.063	53.90	0.9940
		100	0.026	99.66	0.9927	0.016	117.77	0.9938
	MB	50	0.033	49.21	0.9925	0.040	57.18	0.9753
		100	0.032	99.17	0.9960	0.019	115.53	0.9825

Fig. S1 is a fitting diagram of the internal diffusion model of hydroxyapatite composite hydrogel (support information, equation 3). It can be seen that the adsorption process mainly includes two steps, and the curve of the first step does not pass through the origin. According to the model, if it passes through the origin, it is considered that the adsorption of pollutants is two steps working at the same time [31, 32].

3.2.3 Adsorption isotherm and thermodynamics

Langmuir, Freundlich and Dubinin-Radushkevich (D-R) isotherm models are most commonly used in adsorption thermodynamic models (supporting information, equations 4-5). Fig. S2 fitting Langmuir and Freundlich models for hydroxyapatite composite hydrogel to adsorb three pollutants. The adsorption capacity of the composites for the three pollutants increases with the increase of pollutant concentration.

Even if the pollutant concentration (> 200 mg / L) is higher, the materials have higher removal efficiency (> 95%). In addition, when the content of hydroxyapatite increased, the adsorption capacity of hydrogel increased. At 313K, the maximum adsorption capacity of hydroxyapatite composite hydrogel (5%) was 337.68mg/g (Pb), 226.26mg/g (Ni) and 330.46mg/g (MB). In addition, it can be seen from Figure S1 that the fitting result of the adsorption isotherm is more complex with the Langmuir adsorption model (R2>0.98), indicating that the adsorption of the three pollutants by the material is mainly through single-layer adsorption[33, 30].

Table S2-3 and Figure S3 show the fitting results of the adsorption thermodynamics and the Dubinin-Radushkevich adsorption isotherm model[34]. It can be seen that according to the Vanter Hoff equation, the adsorption process of hydroxyapatite hydrogel to the three pollutants is exothermic and spontaneous ($\triangle G < 0$, $\triangle S > 0$) [6]. According to the Dubinin-Radushkevich adsorption isotherm model, E(8.18-11.97) is calculated in the range of 8-16 kJ/mol. It can be determined that the main form of adsorption of the three pollutants by the material is through chemical adsorption [35].

3.2.4 Adsorption mechanism

Different adsorbents have different adsorption mechanisms, such as electrostatic interaction, ion exchange and chelation [36, 37, 21]. The polyvinyl alcohol and acrylamide of the hydrogel contain a large number of electron-rich groups such as carboxyl groups and amino groups that can adsorb pollutants [38].

In order to further prove the mechanism of this study, taking the state before and after the adsorption of lead ions by the hydrogel as an example, X-ray photoelectron spectroscopy was used to test the changes before and after the adsorption of lead ions by the hydrogel (Figure 7). First, from the full spectrum scan, a new peak of Pb4f appears in the material, indicating that lead ions are adsorbed by the material (Figure 6a). Figure 6b shows the precise scanning spectrum of C1s, which can be divided into three peaks: C-C, C-N and C=O[39, 40]. When lead ions are adsorbed, the binding energies of these three peaks all increase to different degrees, indicating that nitrogen and oxygen near carbon are involved in the adsorption process. Figure 6c and Figure 6d correspond to the precise scanning spectra of O1s and N1s, respectively, corresponding to O=C and $-NH_3^+$ at 532.08eV and 399.48eV [41]. After the adsorption process technology, O=C and $-NH_3^+$ The binding energies of the corresponding peaks all appear to increase, indicating that the lone pair electrons in nitrogen form coordination bonds with lead ions, thereby adsorbing lead ions [42].

3.2.5 Comparison with other adsorbents

Hydroxyapatite hydrogel has a high adsorption capacity, but the adsorption capacity cannot be directly compared between adsorbents due to different use conditions. In terms of adsorption capacity, Table S4 summarizes the adsorption capacity of this study and other adsorbents. It can be seen that hydroxyapatite hydrogel has great potential in the field of pollutant removal.

3.2.6 Selective adsorption test and Adsorption Recyclability

In this study, the selective adsorption of materials was tested to deal with the diversity of pollutants in wastewater. The selective adsorption properties of hydrogels were tested by mixed solutions of four metal ions (Pb (II), Cu (II), Zn (II) and Ni (II)). The results are shown in Figure 7. The removal efficiency of lead ion by hydroxyapatite hydrogel is higher than that of the other three (> 80%), followed by copper ion, zinc ion and nickel ion. This shows that the material can not only adsorb a variety of ions in the mixed solution, but also preferentially remove lead ions.

Recyclability is a must-have of the adsorbent. The study conducted 5 adsorption-desorption experiments on hydroxyapatite hydrogel, as shown in Figure 8. After 5 cycles of adsorption-desorption experiments, the removal efficiency of hydroxyapatite hydrogel for both ions and dyes is still greater than 81%. The result meets the requirements of the adsorbent, and the decrease in removal efficiency may be caused by the quality loss of the material, but this does not affect the reusability of the material.

Conclusion

In this study, a hydrogel adsorbent was successfully synthesized, and its adsorption and mechanical properties were studied. The study found that after adding hydroxyapatite to the hydrogel, the compressive strength increased (the maximum increase was 37.1%), the swelling performance decreased, and the maximum adsorption capacity of the hydrogel increased by about 10%. Finally, this study can be complicated It removes heavy metal ions and dyes in a high-quality environment, and can be reused many times. The materials used in the research are low in cost and short in process flow, which has great potential for the treatment of polluted wastewater.

Declarations

Funding: This work was supported by the Natural Science Foundation of Tianjin City [18JCQNJC03400]; the National Natural Science Foundation of China [51503145, 11702187]; the Natural Science Foundation of Fujian Province [2018J01504, 2018J01505];

References

[1] Macías-García A, Corzo MG, Domínguez MA, Franco MA, Naharro JM. Study of the adsorption and electroadsorption process of Cu (II) ions within thermally and chemically modified activated carbon. Journal of Hazardous Materials. 2017;328:46-55.

[2] Zhu F, Li L, Xing J. Selective adsorption behavior of Cd (II) ion imprinted polymers synthesized by microwave-assisted inverse emulsion polymerization: Adsorption performance and mechanism. Journal of Hazardous Materials. 2017;321:103-10.

[3] Al-Rashdi B, Johnson D, Hilal N. Removal of heavy metal ions by nanofiltration. Desalination. 2013;315:2-17.

[4] Anitha K, Namsani S, Singh JK. Removal of heavy metal ions using a functionalized single-walled carbon nanotube: a molecular dynamics study. The Journal of Physical Chemistry A. 2015;119(30):8349-58.

[5] Gogoi N, Barooah M, Majumdar G, Chowdhury D. Carbon dots rooted agarose hydrogel hybrid platform for optical detection and separation of heavy metal ions. ACS applied materials & interfaces. 2015;7(5):3058-67.

[6] Xu R, Zhou G, Tang Y, Chu L, Liu C, Zeng Z, et al. New double network hydrogel adsorbent: Highly efficient removal of Cd (II) and Mn (II) ions in aqueous solution. Chemical Engineering Journal. 2015;275:179-88.

[7] Phetphaisit CW, Yuanyang S, Chaiyasith WC. Polyacrylamido-2-methyl-1-propane sulfonic acid-grafted-natural rubber as bio-adsorbent for heavy metal removal from aqueous standard solution and industrial wastewater. Journal of Hazardous Materials. 2016;301:163-71.

[8] Repo E, Warchoł JK, Bhatnagar A, Mudhoo A, Sillanpää M. Aminopolycarboxylic acid functionalized adsorbents for heavy metals removal from water. Water Research. 2013;47(14):4812-32.

[9] Tan L, Wang S, Du W, Hu T. Effect of water chemistries on adsorption of Cs (I) onto graphene oxide investigated by batch and modeling techniques. Chemical Engineering Journal. 2016;292:92-7.

[10] Echeverria C, Fernandes SN, Godinho MH, Borges JP, Soares PI. Functional stimuli-responsive gels: Hydrogels and microgels. Gels. 2018;4(2):54.

[11] Liao H, Liu Y, Wang Q, Duan W. Preparation and properties of a poly (vinyl alcohol) hydrogel-melamine formaldehyde foam composite. Polymer Composites. 2019;40(5):2067-75.

[12] Anjum S, Gurave P, Badiger MV, Torris A, Tiwari N, Gupta B. Design and development of trivalent aluminum ions induced self-healing polyacrylic acid novel hydrogels. Polymer. 2017;126:196-205.

[13] Martín C, Merino S, González-Domínguez JM, Rauti R, Ballerini L, Prato M, et al. Graphene improves the biocompatibility of polyacrylamide hydrogels: 3D polymeric scaffolds for neuronal growth. Scientific Reports. 2017;7(1):1-12.

[14] Chu L, Liu C, Zhou G, Xu R, Tang Y, Zeng Z, et al. A double network gel as low cost and easy recycle adsorbent: highly efficient removal of Cd (II) and Pb (II) pollutants from wastewater. Journal of Hazardous Materials. 2015;300:153-60.

[15] Ma J, Liu Y, Ali O, Wei Y, Zhang S, Zhang Y, et al. Fast adsorption of heavy metal ions by waste cotton fabrics based double network hydrogel and influencing factors insight. Journal of Hazardous Materials. 2018;344:1034-42.

[16] Zhou G, Liu C, Chu L, Tang Y, Luo S. Rapid and efficient treatment of wastewater with high-concentration heavy metals using a new type of hydrogel-based adsorption process. Bioresource technology. 2016;219:451-7.

[17] Chen Y, Peng J, Xiao H, Peng H, Bu L, Pan Z, et al. Adsorption behavior of hydrotalcite-like modified bentonite for Pb2+, Cu2+ and methyl orange removal from water. Applied Surface Science. 2017;420:773-81.

[18] Liu X, Cheng C, Xiao C, Shao D, Xu Z, Wang J, et al. Polyaniline (PANI) modified bentonite by plasma technique for U (VI) removal from aqueous solution. Applied Surface Science. 2017;411:331-7.

[19] Nayak AK. Hydroxyapatite synthesis methodologies: an overview. International Journal of ChemTech Research. 2010;2(2):903-7.

[20] Abollino O, Giacomino A, Malandrino M, Mentasti E. Interaction of metal ions with montmorillonite and vermiculite. Applied Clay Science. 2008;38(3-4):227-36.

[21] Sellaoui L, Soetaredjo FE, Ismadji S, Bonilla-Petriciolet A, Belver C, Bedia J, et al. Insights on the statistical physics modeling of the adsorption of Cd2+ and Pb2+ ions on bentonite-chitosan composite in single and binary systems. Chemical Engineering Journal. 2018;354:569-76.

[22] Abd Jelil R. A review of low-temperature plasma treatment of textile materials. Journal of Materials Science. 2015;50(18):5913-43.

[23] Sun J, Li L, Kong Q, Zhang Y, Zhao P, Ge S, et al. Mimic peroxidase-transfer enhancement of photoelectrochemical aptasensing via CuO nanoflowers functionalized lab-on-paper device with a controllable fluid separator. Biosensors and Bioelectronics. 2019;133:32-8.

[24] Zhao G, Li J, Ren X, Chen C, Wang X. Few-layered graphene oxide nanosheets as superior sorbents for heavy metal ion pollution management. Environmental science & technology. 2011;45(24):10454-62.

[25] Daelemans L, Steyaert I, Schoolaert E, Goudenhooft C, Rahier H, De Clerck K. Nanostructured hydrogels by blend electrospinning of polycaprolactone/gelatin nanofibers. Nanomaterials. 2018;8(7):551.

[26] Li T-T, Zhang Y, Ren H-T, Peng H-K, Lou C-W, Lin J-H. Two-step strategy for constructing hierarchical pore structured chitosan–hydroxyapatite composite scaffolds for bone tissue engineering. Carbohydrate Polymers. 2021;260:117765.

[27] Liu M, Chen C, Hu J, Wu X, Wang X. Synthesis of magnetite/graphene oxide composite and application for cobalt (II) removal. The Journal of Physical Chemistry C. 2011;115(51):25234-40.

[28] Cabaniss SE. Forward modeling of metal complexation by NOM: II. Prediction of binding site properties. Environmental science & technology. 2011;45(8):3202-9.

[29] Jiang M-q, Wang Q-p, Jin X-y, Chen Z-l. Removal of Pb (II) from aqueous solution using modified and unmodified kaolinite clay. Journal of Hazardous Materials. 2009;170(1):332-9.

[30] Sari A, Tuzen M, Citak D, Soylak M. Equilibrium, kinetic and thermodynamic studies of adsorption of Pb (II) from aqueous solution onto Turkish kaolinite clay. Journal of Hazardous Materials. 2007;149(2):283-91.

[31] Dou X, Mohan D, Pittman Jr CU. Arsenate adsorption on three types of granular schwertmannite. Water research. 2013;47(9):2938-48.

[32] Vandenbossche M, Vezin H, Touati N, Jimenez M, Casetta M, Traisnel M. Cysteine-grafted nonwoven geotextile: A new and efficient material for heavy metals sorption–Part B. Journal of environmental management. 2014;143:99-105.

[33] Foo KY, Hameed BH. Insights into the modeling of adsorption isotherm systems. Chemical Engineering Journal. 2010;156(1):2-10.

[34] Dada A, Olalekan A, Olatunya A, Dada O. Langmuir, Freundlich, Temkin and Dubinin–Radushkevich isotherms studies of equilibrium sorption of Zn2+ unto phosphoric acid modified rice husk. IOSR Journal of Applied Chemistry. 2012;3(1):38-45.

[35] Liu Y, You CC, Li B. Synthesis and molecular recognition of novel oligo (ethylenediamino) bridged bis (β-cyclodextrin) s and their copper (II) complexes: enhanced molecular binding ability and selectivity by multiple recognition. Chemistry–A European Journal. 2001;7(6):1281-8.

[36] Bergaoui M, Nakhli A, Benguerba Y, Khalfaoui M, Erto A, Soetaredjo FE, et al. Novel insights into the adsorption mechanism of methylene blue onto organo-bentonite: Adsorption isotherms modeling and molecular simulation. Journal of Molecular Liquids. 2018;272:697-707.

[37] Huang Z, Li Y, Chen W, Shi J, Zhang N, Wang X, et al. Modified bentonite adsorption of organic pollutants of dye wastewater. Materials Chemistry and Physics. 2017;202:266-76.

[38] Pakdel PM, Peighambardoust SJ. A review on acrylic based hydrogels and their applications in wastewater treatment. Journal of environmental management. 2018;217:123-43.

[39] Qi H-X, Zhai S-R, Wang Z-Z, Zhai B, An Q-D. Designing recyclable Cu/ZrSBA-15 for efficient thiophene removal. Microporous and Mesoporous Materials. 2015;217:21-9.

[40] Zendehdel M, Zamani F. MCM-41-supported NNO type Schiff base complexes: a highly selective heterogeneous nanocatalyst for esterification, Diels–Alder and aldol condensation. Journal of Porous Materials. 2017;24(5):1263-77.

[41] Sun J, Cui K, Li L, Zhang L, Yu J. Visible-light-driven renewable photoelectrochemical/synchronous visualized sensing platform based on Ni: FeOOH/BiVO4 photoanode and enzymatic cascade

amplification for carcinoembryonic antigen detection. Sensors and Actuators B: Chemical. 2020;304:127301.

[42] Ma W, Ding Y, Zhang M, Gao S, Li Y, Huang C, et al. Nature-inspired chemistry toward hierarchical superhydrophobic, antibacterial and biocompatible nanofibrous membranes for effective UV-shielding, self-cleaning and oil-water separation. Journal of Hazardous Materials. 2020;384:121476.

Figures

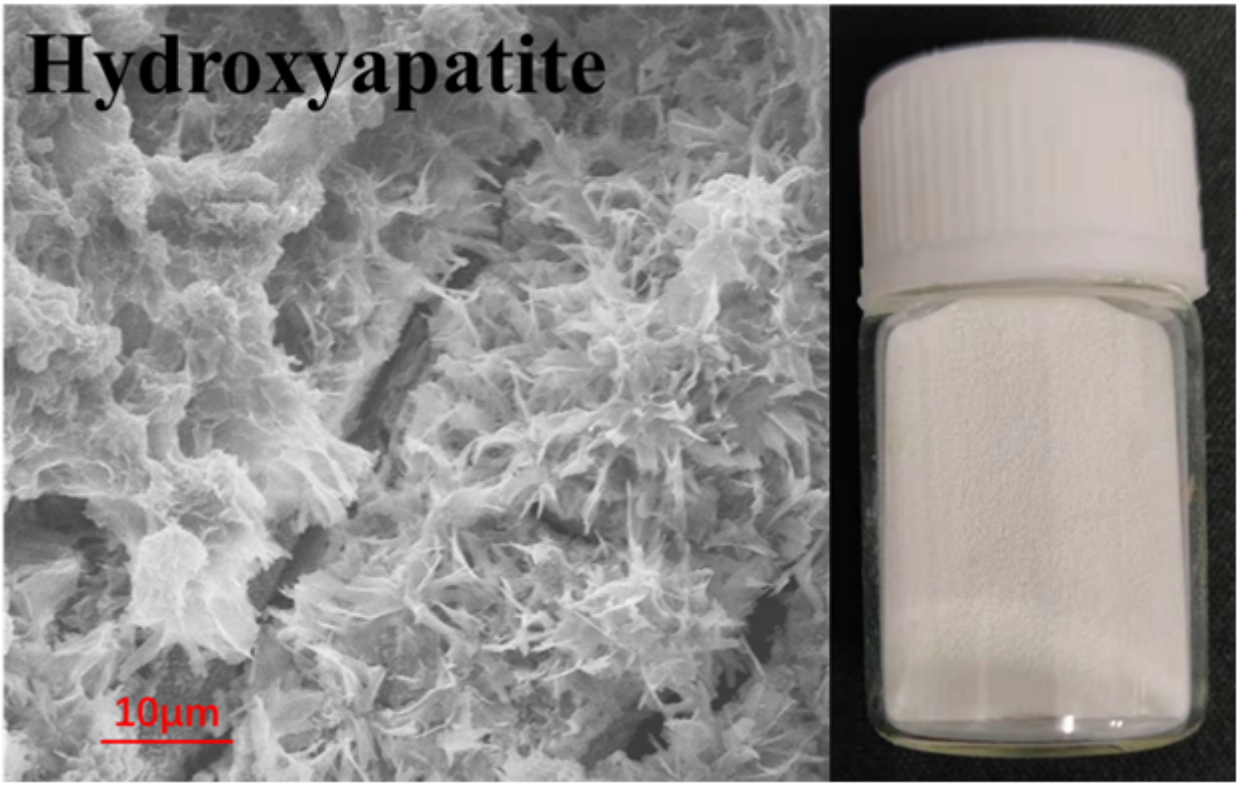

Figure 1

Physical map of clay

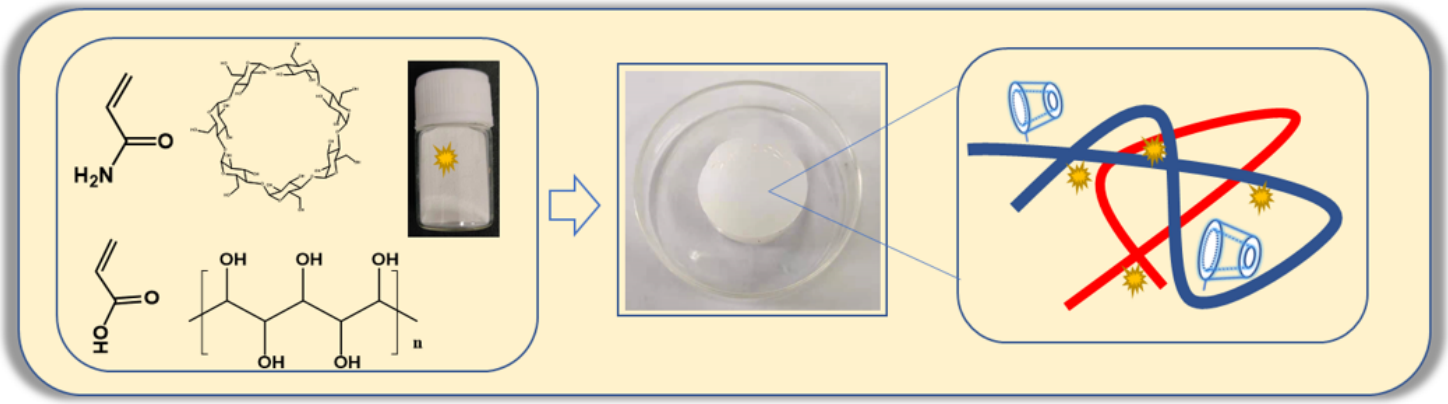

Figure 2

Preparation process of hydrogel

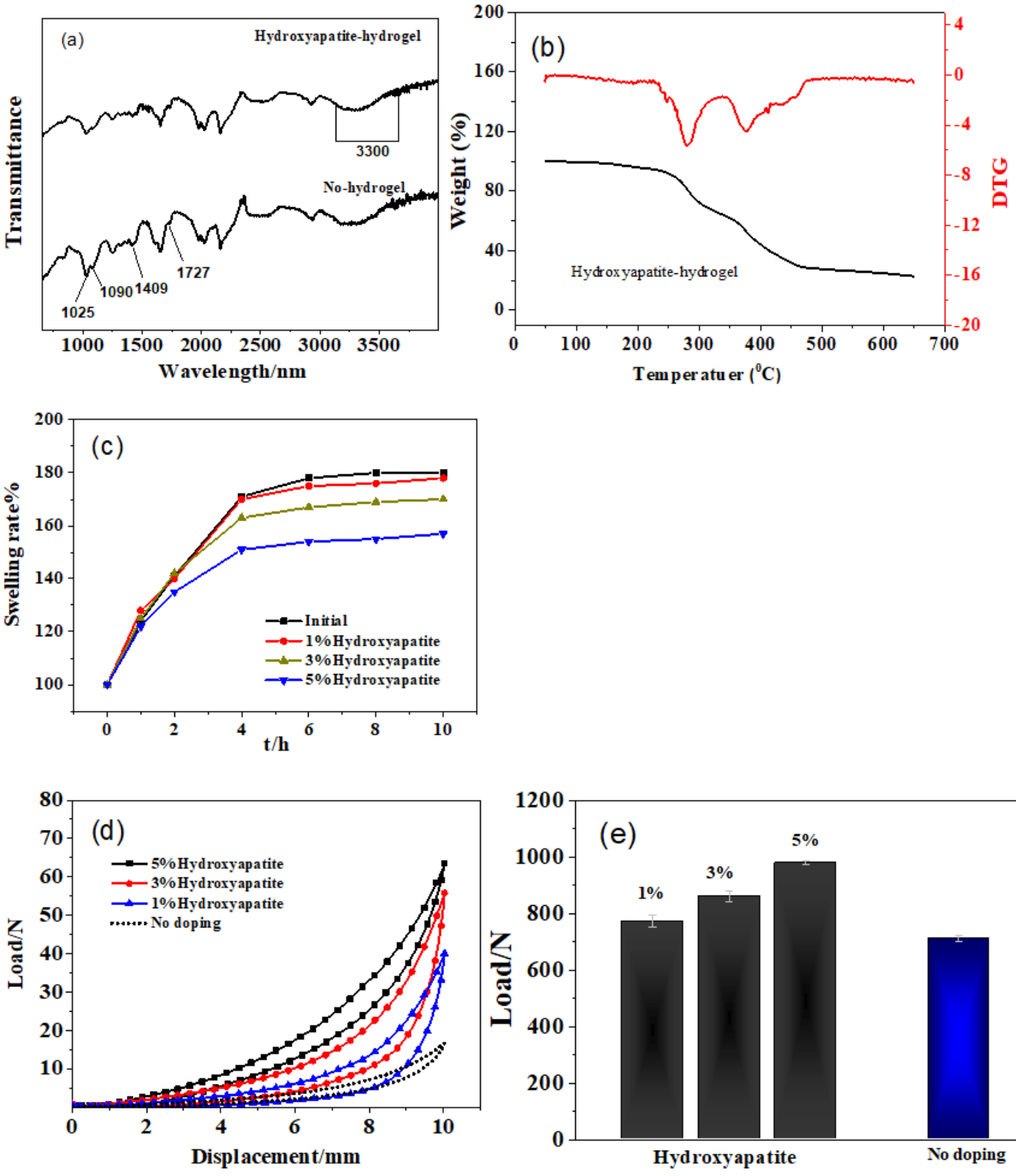

Figure 3

Infrared spectrogram(a) and thermogravimetric analysis diagram(b) of hydrogel; schematic diagram of swelling of hydrogel with different hydroxyapatite content(c); The compression rebound curve and maximum compression force value(d) of hydroxyapatite hydrogel at 50% deformation(e)

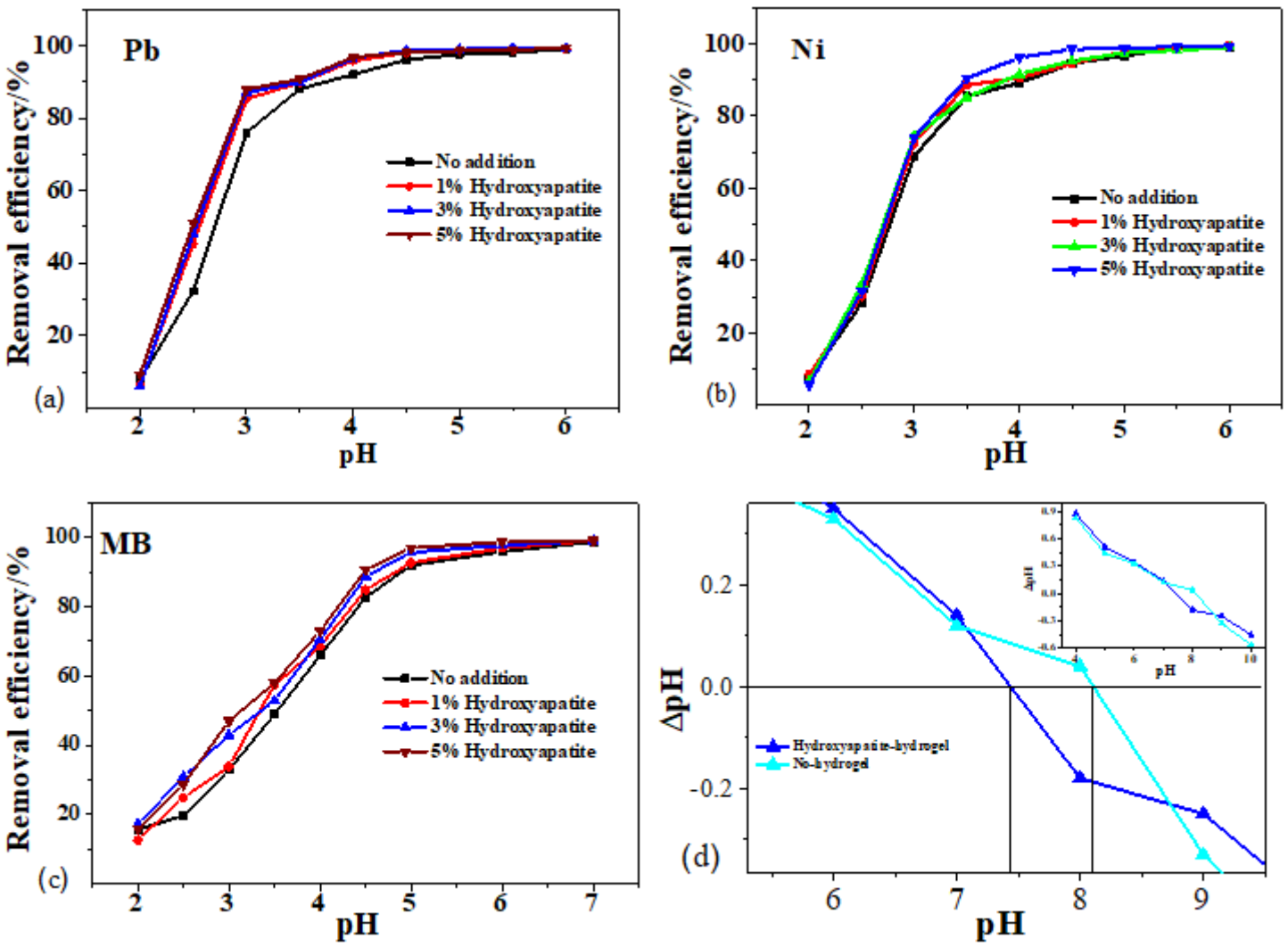

Figure 4

The effect of pH changes on the adsorption performance of Hydroxyapatite composite hydrogel.C0=100 mg/L, m/V=1g/L, T=298K.

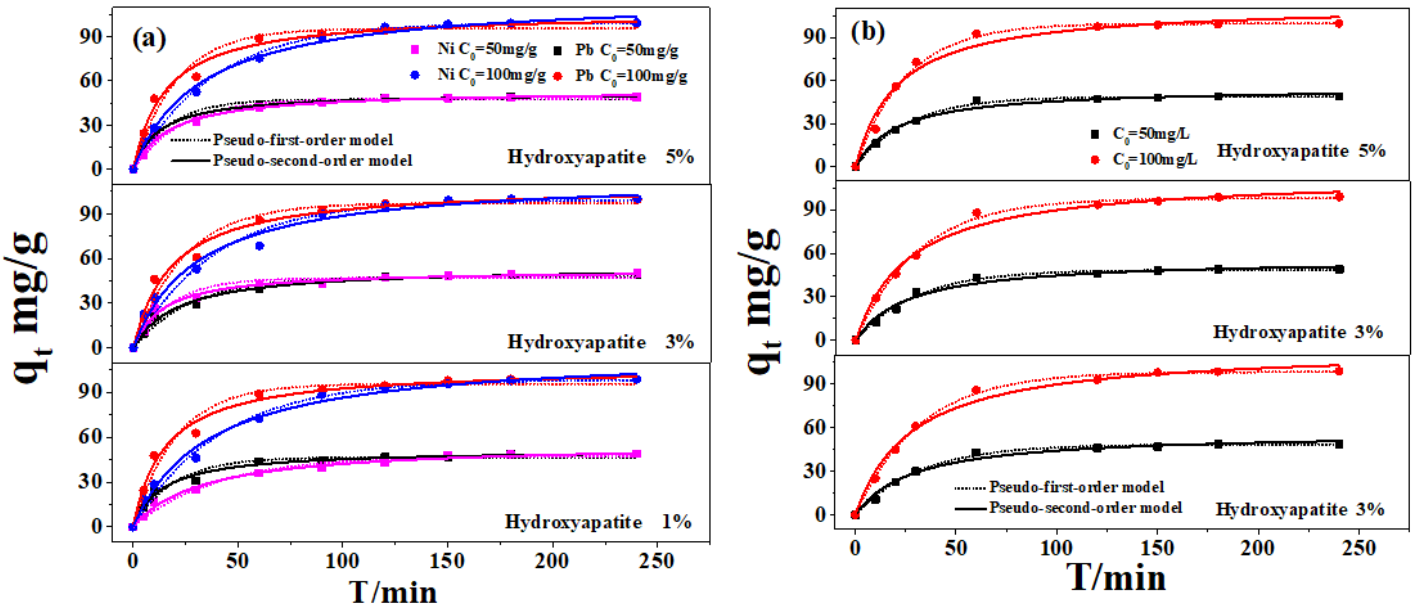

Figure 5

Sorption kinetics of Pb(II) and Ni(II) on hydroxyapatite composite hydrogel (a), Sorption kinetics of MB on hydroxyapatite composite hydrogel (b),. C0 = 50 mg/L or 100 mg/L, T = 303 K, m/V = 1 mg/mL, pH=5

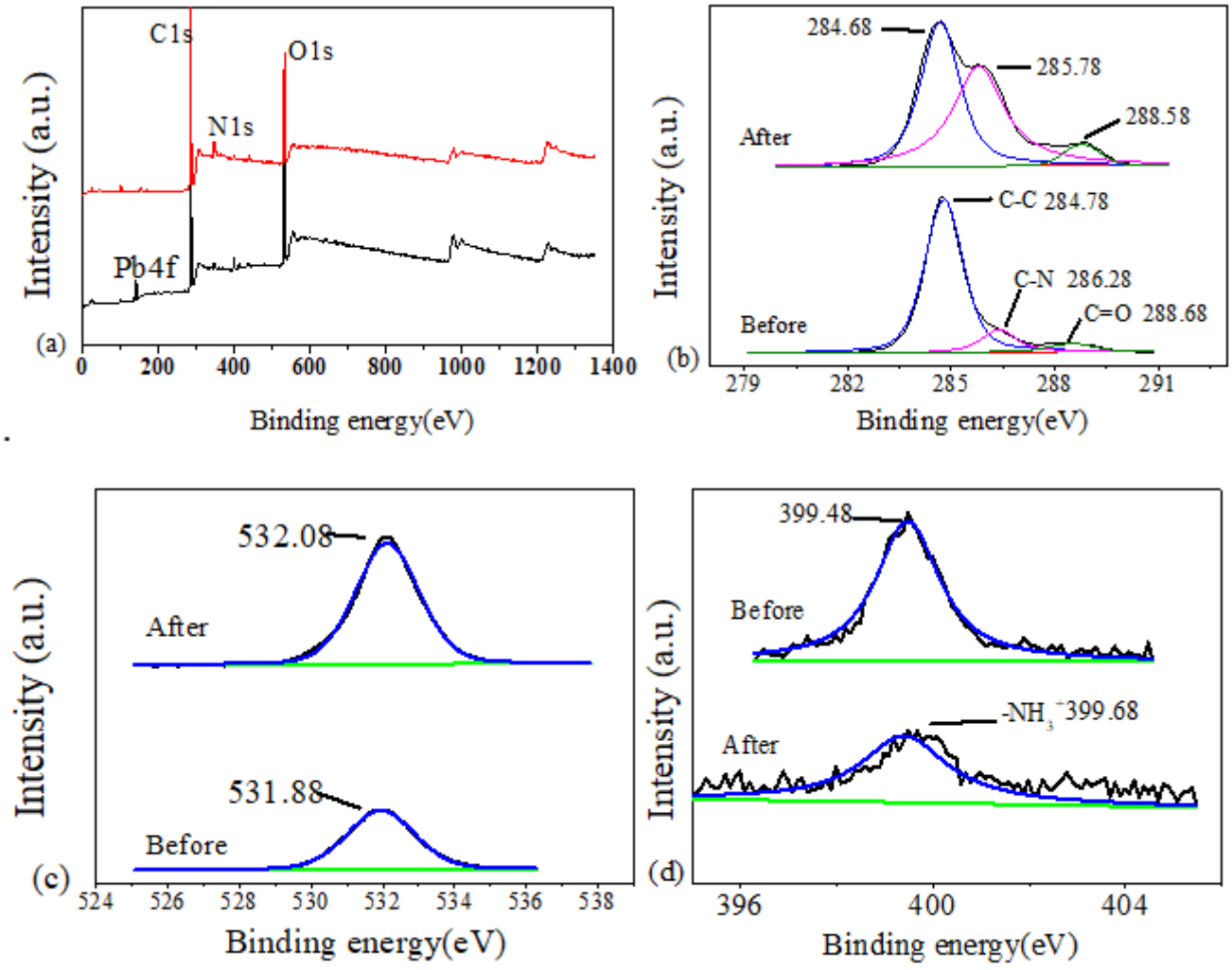

Figure 6

XPS spectra of hydroxyapatite composite hydrogel before and after the adsorption of lead ions. (a) Full spectrum scan;(b) C1s peaks; (c) O1s peaks; (d) N1speaks

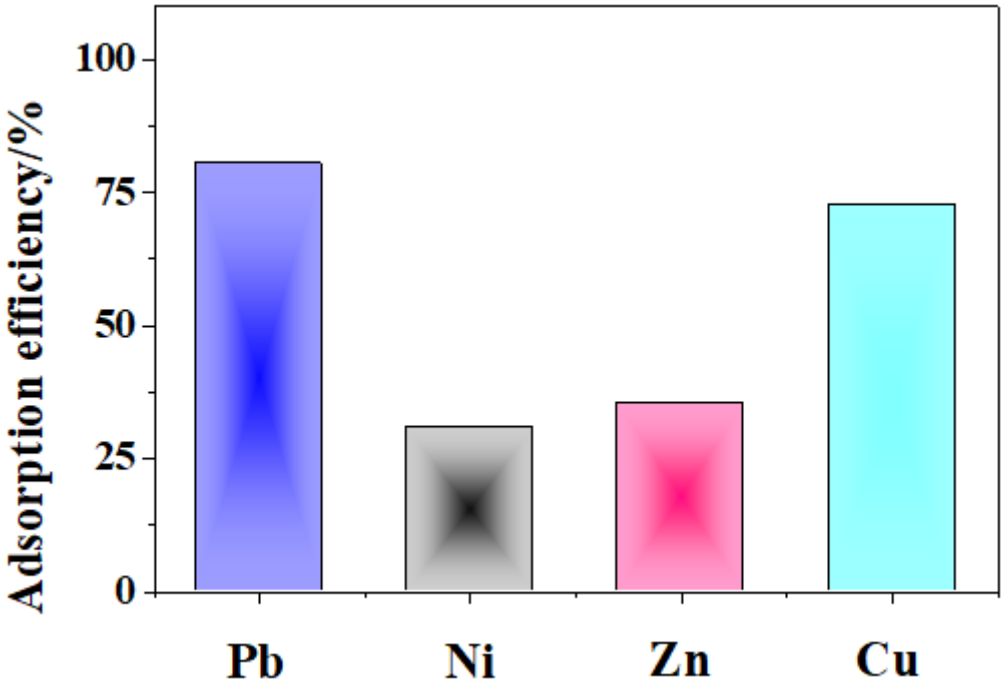

Figure 7

The adsorption efficiency of composite materials for mixed ions. pH=5，T=298K，C0=100mg/L.

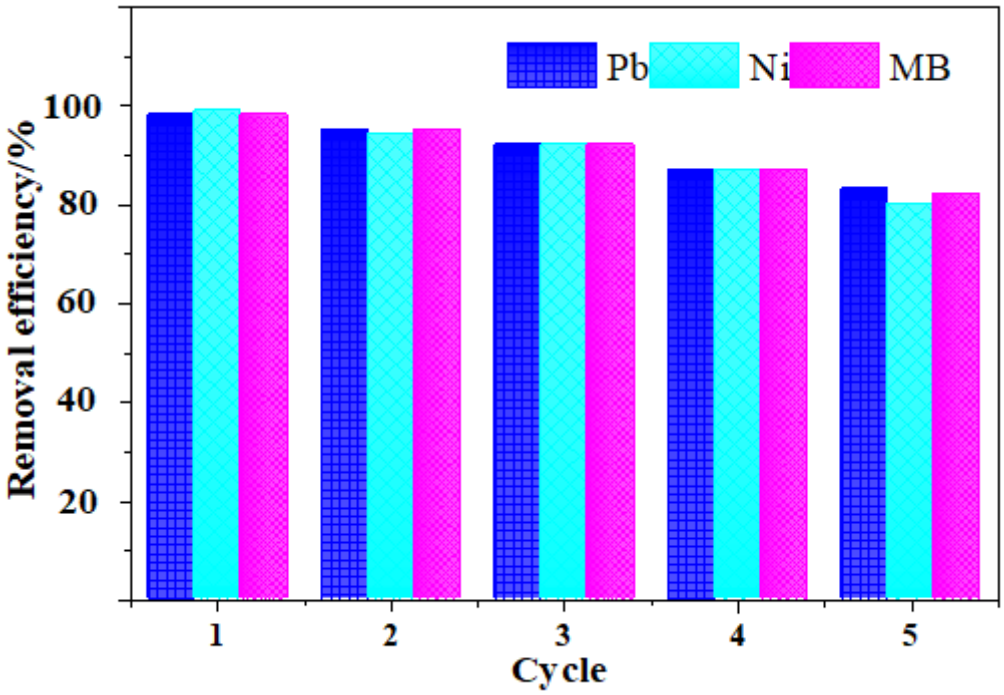

Figure 8

Composite material circulation adsorption test. T = 313 K, m/V = 1 g/L, pH = 5, t=6h. C0=100mg/L

Supplementary Files

This is a list of supplementary files associated with this preprint. Click to download.

- Supportinginformation.docx